Photodegradation of C.I. reactive red 2 in UV/TiO$_2$–In$_2$O$_3$–C–N and UV/TiO$_2$–In$_2$O$_3$–S–N systems

Jui-Tai Wu · Chao-Yin Kuo · Chung-Hsin Wu

Abstract In this study, the sol–gel method is utilized to produce TiO$_2$–In$_2$O$_3$ composite (Ti–In). The generated Ti–In was separately co-doped with C–N and S–N to form novel TiO$_2$–In$_2$O$_3$–C–N (Ti–In–C–N) and TiO$_2$–In$_2$O$_3$–S–N (Ti–In–S–N). The sources of N, C and S dopants were urea, powder activated carbon and Na$_2$S$_2$O$_3$. The dye C.I. reactive red 2 (RR2) was used as a model compound that was exposed to various composites and its removal by photocatalytic degradation and adsorption was measured. The percentage of anatase phase in Ti–In–C–N and Ti–In–S–N exceeded that in Ti–In; conversely, the particle diameter and band gap energy of Ti–In exceeded those of Ti–In–C–N and Ti–In–S–N. Bonds of Ti–O–N, Ti–N–O and Ti–O–C were detected in Ti–In–C–N and bonds of Ti–O–N, Ti–N–O and Ti–O–S were found in Ti–In–S–N. The pseudo-first order RR2 removal rate constants in UV/Ti–In, UV/Ti–In–C–N and UV/Ti–In–S–N were 0.43, 1.68 and 1.70 h^{-1}, in order. The specific oxygen uptake rates of the RR2 effluent in UV/Ti–In, UV/Ti–In–C–N and UV/Ti–In–S–N were determined to be 4.4, 7.3 and 5.3 mg O$_2$/g-MLVSS h. Ti–In–C–N and Ti–In–S–N were more effective in decolorizing and detoxifying RR2 than was their parent Ti–In.

Keywords TiO$_2$ · In$_2$O$_3$ · C–N co-doping · S–N co-doping · Photodegradation

J.-T. Wu · C.-H. Wu (✉)
Department of Chemical and Materials Engineering, National Kaohsiung University of Applied Sciences, 415 Chien Kung Road, Kaohsiung, Taiwan
e-mail: wuch@kuas.edu.tw

C.-Y. Kuo
Department of Environmental and Safety Engineering, National Yunlin University of Science and Technology, 123 University Road, Sec. 3, Douliou, Yunlin, Taiwan

Introduction

Advanced oxidation refers to a set of chemical treatment procedures for removing organic and inorganic materials from wastewater by oxidation. Photocatalysis using a nanosized metal oxide semiconductor is regarded as one of the most effective and simplest ways to mitigate environmental pollution that is caused by humans. Titanium dioxide (TiO_2) is currently considered to be the most promising photocatalyst because of its chemical and biological stability, high abundance and non-toxicity. The photocatalytic degradation of pollutants in water has been successfully performed using a suspension of TiO_2. The generally accepted mechanisms of the photodegradation of organics by UV/TiO_2 are as follows [1]. Photogenerated holes are formed when TiO_2 particles are irradiated by UV light. Hydroxyl radicals are produced by the oxidation of OH^- or H_2O by these photogenerated holes, and are primarily responsible for the destruction of the organic species. Oxygen is used as an efficient electron trap to prevent the recombination of photogenerated electrons and holes. If the amount of available oxygen is limited, then the rapid recombination of photogenerated electrons and holes in TiO_2 reduces the efficiency of the photocatalytic reactions.

A different method for preparing photocatalytic TiO_2 efficiently involves coupling it with other semiconductor oxides, such as CdSe [2], SnO_2 [3, 4], WO_3 [4], and In_2O_3 [5–7]. These composite systems demonstrate considerably enhanced photocatalytic performance in the degradation of pollutants, as the composite facilitates charge transfer and suppresses the recombination of electron–hole pairs in the photocatalysts systems. Coupling In_2O_3 with TiO_2 enables the transfer of the photogenerated electrons from the surface of In_2O_3 to the conduction band of TiO_2 because the band gap of In_2O_3 (2.64 eV) is lower than that of TiO_2 (2.95 eV) and the conduction band of In_2O_3 (-0.63 eV vs. NHE) is higher than that of TiO_2 (-0.4 eV vs. NHE). This process results in the effective capture of photogenerated electrons and retardation of the recombination of photogenerated electron–hole pairs [7, 8]. Various studies have demonstrated that the photocatalytic activity of TiO_2–In_2O_3 composite (Ti–In) exceeds that of In_2O_3 and TiO_2 [5, 6].

Various metal and nonmetal ions have been doped into photocatalysts to reduce the recombination of photogenerated electrons and holes in them and to increase their absorption of light. However, metal ion-doped photocatalysts have some serious drawbacks, such as thermal instability and the metal centers acting as electron traps, reducing photocatalytic efficiency [9]. Sojic et al. [10] showed that nonmetals are more efficient dopants than metals. Accordingly, doping nonmetal ions into photocatalysts has recently attracted considerable attention. Nonmetal-doped forms of TiO_2, including C-doped [11–13], N-doped [10–12] and S-doped TiO_2 [12, 14–16], has been found to exhibit superior photocatalytic activity because C, N and S atoms can effectively narrow the energy band gap of TiO_2. Moreover, C–N [11] and S–N co-doped TiO_2 [17, 18] have been investigated and co-doped TiO_2 has been found to have a higher photocatalytic activity than single-doped TiO_2 [11, 18].

Ma et al. [8] demonstrated that the photocatalytic activity of Pt/Ti–In exceeded that of Ti–In because the separation of the photogenerated electron–hole pairs in the former is more efficient, owing to the incorporation of In_2O_3 and Pt into the TiO_2

framework. Ag/Ti–In has been found to exhibit a similar enhancement [19]. However, to the best of our knowledge, the photocatalytic activities of Ti–In that is co-doped with nonmetal dopants have not been examined. In this study, the Ti–In photocatalyst was synthesized via the sol–gel method, doped separately with C and S, and finally the C-doped and S-doped Ti–In were calcined with urea to form C–N co-doped and S–N co-doped Ti–In. To determine the photocatalytic activities of C–N-co-doped and S–N-co-doped Ti–In, their removal of a common azo dye, C.I. reactive red 2 (RR2), was studied. The objectives of this study are (i) to prepare novel C–N-co-doped Ti–In (abbreviated as Ti–In–C–N) and S–N-co-doped Ti–In (Ti–In–S–N), (ii) to characterize the surface properties of Ti–In–C–N and Ti–In–S–N, (iii) to determine changes associated with the adsorption of RR2 onto Ti–In–C–N and Ti–In–S–N, and (iv) to evaluate the photocatalytic activities of the doped Ti–In–C–N and Ti–In–S–N in decolorizing RR2, relative to that of their parent Ti–In.

Materials and methods

Materials

In this investigation, the sources of Ti and In are $TiCl_4$ (Acros) and $InCl_3$ (Alfa Aesar). The sources of N, C and S dopants were urea (Katayama), powder activated carbon (PAC) (Katayama) and $Na_2S_2O_3$ (Merck. The parent compound, RR2, was purchased from Sigma Aldrich. Its formula, molecular weight, and maximum light absorption wavelength were $C_{19}H_{10}Cl_2N_6Na_2O_7S_2$, 615 g/mol, and 538 nm. The pH of the solution was adjusted by adding 0.1 M HNO_3 (Merck) or NaOH (Merck). All compounds were used as received (without further purification), and all solutions were prepared using deionized water (Milli-Q) and reagent-grade chemicals.

Preparation of Ti–In, Ti–In–C–N and Ti–In–S–N

Ti–In was prepared with a Ti/In mole ratio of 54 using the sol–gel method, as previously described [7]. The molar ratios of Ti/C and Ti/S in Ti–In–C–N and Ti–In–S–N were both 7.5; the molar ratios of Ti/N in both Ti–In–C–N and Ti–In–S–N were both 0.07.

To prepare Ti–In–C–N and Ti–In–S–N, C-doped Ti–In (Ti–In–C) and S-doped Ti–In (Ti–In–S) were first produced. To prepare the Ti–In–C, PAC (0.184 g) was first mixed with HCl (20 mL; 0.65 M) and the mixture was placed in an ultrasonic bath for 10 min; then this solution was added $InCl_3$ (0.4805 g; 99.9 %) and $TiCl_4$ (13 mL; 98 %). The pH of the solution was adjusted to pH 8 by adding NH_4OH solution (28 %), forming a solid precipitate. This precipitate was collected by filtration and washed repeatedly using distilled water; it was dried at 110 °C for 24 h and then calcined at 450 °C for 2 h to yield the Ti–In–C. To prepare Ti–In–S, PAC was replaced with $Na_2S_2O_3$ (1.212 g) and the other steps were the same as those used to prepare Ti–In–C. To prepare Ti–In–C–N (or Ti–In–S–N), 2.5 g Ti–In–C (or Ti–In–S) and urea (12.5 g) were thoroughly mixed and the mixture was calcined at 450 °C for 2 h.

Characterization of Ti–In–C–N and Ti–In–S–N

The crystalline structures of various photocatalysts were analyzed by X-ray diffraction (XRD) (Bruker D8 SSS, Germany). The XRD patterns were recorded over 2θ values of 10–90°, with an accelerating voltage and applied current of 40 kV and 30 mA, respectively. Diffuse reflectance UV–Vis spectra of the photocatalysts were obtained using a UV–Vis spectrophotometer (JAS.CO-V670, Japan) and these were used to calculate the band gap energies. Specific surface areas of the samples were determined by the BET method from the nitrogen adsorption isotherms that were obtained using a Micrometrics ASAP 2020 apparatus. X-ray photoelectron spectroscopy (XPS) measurements were made using a PHI Quantum 5000 XPS system (USA) with a monochromatic Al K_α source and a charge neutralizer.

Decolorization of RR2

Experiments were performed using 0.2 g/L of each photocatalyst, with [RR2] = 20 mg/L, at pH 3 and 25 °C. Decolorization experiments were conducted in a 3 L hollow cylindrical glass reactor, illuminated by an 8 W UV lamp (254 nm, Philips) with a light intensity of 1.12 W/m^2 that was placed inside a quartz tube. Adsorption experiments were performed in the dark. The reaction medium was continuously stirred at 300 rpm to maintain the suspension. Aliquots each with a volume of 10 mL were withdrawn from the reactor at intervals to monitor reaction progress. Following sampling, solids were separated by filtration using a 0.22 μm filter (Millipore), and the RR2 that remained in the filtrate was analyzed by measuring absorbance at 538 nm using a spectrophotometer (Hitachi U-5100, Japan).

Tests of specific oxygen uptake rate (SOUR)

The biodegradability of RR2 effluent was evaluated by performing a SOUR test. Activated sludge was collected from a sewage treatment plant in Kaohsiung. Before testing, the activated sludge was aerated for 24 h. The concentration of mixed liquor volatile suspended solids (MLVSS) in activated sludge was measured to be 3.5 g/L. The SOUR (mg O_2/g-MLVSS h) of aerobic microorganisms was measured for the RR2 effluent (after 180 min reaction and separated the suspended photocatalyst) to be the biodegradability index in the UV/Ti–In, UV/Ti–In–C–N and UV/Ti–In–S–N systems. SOURs were determined by dividing abatement rates in dissolved oxygen (DO) to MLVSS values.

Results and discussion

Characteristics of the surface of prepared photocatalysts

Fig. 1 displays the XRD patterns of Ti–In, Ti–In–C–N and Ti–In–S–N. The anatase peaks were at 25.4° and 48.2°. The peaks at 27.5°, 36.2°, 41.3°, 54.4°, and 69.2° were attributable to rutile crystal phases. The peaks at 21.5°, 30.6°, 35.5°, 51.0°, and

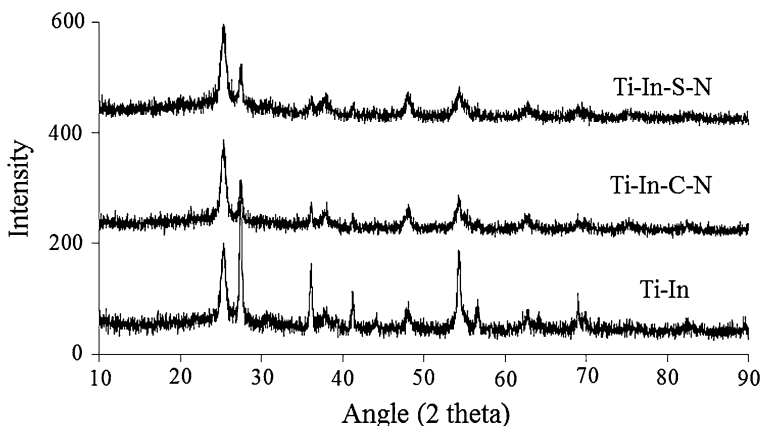**Fig. 1** XRD patterns of Ti–In, Ti–In–C–N and Ti–In–S–N

Table 1 Parameters of surface properties for various photocatalysts

Photocatalysts	Anatase (%)	Rutile (%)	Diameter (nm)	Band gap (eV)	BET (m²/g)	k (h⁻¹)
Ti–In	30	70	57	2.97	35.7	0.43 (0.999)
Ti–In–C–N	63	37	33	2.86	35.6	1.68 (0.988)
Ti–In–S–N	64	36	33	2.82	42.3	1.70 (0.982)

(): denoted the value of R^2

60.7° were attributable to In_2O_3. No pattern included any In_2O_3-derived, N-derived, S-derived, or C-derived peaks.

The anatase content was determined from the integrated intensity of the anatase diffraction peak at $2\theta = 25.4°$, I_A, and the rutile content was determine from the rutile diffraction peak at $2\theta = 27.5°$, I_R, using Eq. 1 below [20]. From the XRD patterns, the crystalline size was calculated using the Scherrer equation, Eq. 2 [21]:

$$\text{Anatase } (\%) = \frac{1}{1 + 12.6\frac{I_A}{I_R}} \times 100 \qquad (1)$$

$$D = \frac{0.9\lambda}{\beta \cos\theta} \qquad (2)$$

Here, D represents the crystalline size (nm); λ is the wavelength of the X-rays (0.15418 nm); β is the line-width at the half maximum of the anatase peak at $2\theta = 25.4°$ or of the rutile peak at $2\theta = 27.5°$, and θ is the diffraction angle (°). Table 1 lists the surface properties of various photocatalysts. The surface areas followed the order Ti–In–S–N > Ti–In ≒ Ti–In–C–N. The percentage of anatase phase in Ti–In–C–N and Ti–In–S–N exceeded that in Ti–In. Clearly, C–N and S–N co-doping in Ti–In inhibited the conversion of TiO_2 from anatase to rutile. This

retardation of phase transformation may be due to stabilization of the anatase phase by surrounding N ions via formation of Ti–O–N bonds. Anatase is regarded as the photoactive form of TiO_2, whereas rutile exhibits a low photocatalytic activity. Hurum et al. [22] proposed that electron-trapping sites are more stable in anatase than in rutile, so anatase exhibits greater photocatalytic activity. Accordingly, C–N and S–N co-doping in Ti–In may improve the photocatalytic activity of Ti–In. Additionally, C–N and S–N co-doping in Ti–In reduced the particle diameter, suggesting that the C–N and S–N co-doping retard the agglomeration of Ti–In crystals. Liu et al. [16] indicated that the doping with S effectively inhibited the growth of TiO_2 crystalls and Chen et al. [11] that doping with N had a similar effect. Li et al. [23] also demonstrated that carbon acts as a barrier that controls the growth of TiO_2 powder and prevents its agglomeration.

The band gap energy of Ti–In exceeded those of Ti–In–C–N and Ti–In–S–N (Table 1). N-doping was effective in reducing the band gap of TiO_2 by creating an isolated N_{2p} narrow band above the O_{2p} valence, by the incorporation of N atoms into the TiO_2 lattice [24]. The reduction of the band gap of C-doped TiO_2 was attributed to the formation of Ti–O–C bonds [25]. C–N co-doping generated the intragap localized state of C_{2p} and N_{2p} above the valence band gap of TiO_2. Therefore, electrons were promoted from the valence band to the conduction band, leaving holes behind [26]. The role of S in Ti–In–S–N was same as that of C in Ti–In–C–N; therefore, co-doping of C–N and S–N in Ti–In reduced the band gap energy.

XPS was utilized to determine the chemical compositions of the photocatalysts. Fig. 2a–e display the XPS spectra of Ti_{2p}, In_{3d}, O_{1s}, C_{1s}, and N_{1s} for Ti–In–C–N. The $Ti_{2p3/2}$ and $Ti_{2p1/2}$ spin-orbital-splitting photoelectrons were observed at binding energies of 455.7–458.8 and 462.1–464.5 eV [26–28]. The binding energy of the $Ti_{2p3/2}$ and $Ti_{2p1/2}$ spin-orbital-splitting photoelectrons in Ti–In–C–N was 458.2 and 463.9 eV (Fig. 2). These binding energies are close to those reported for Ti^{4+} in TiO_2 [29]. The $In_{3d5/2}$ and $In_{3d3/2}$ spin-orbital splitting photoelectrons were observed at binding energies of 443.9–445 [19, 28, 30, 31] and 451.5–452.0 eV [19, 28, 30]. The binding energy of the $In_{3d5/2}$ and $In_{3d3/2}$ spin-orbital-splitting photoelectrons of Ti–In–C–N was 444.3 and 451.9 eV (Fig. 2b). Peaks at 528.5–529.5 [26, 28, 32] and 529.6–531.0 eV [27, 30, 31] were assigned to O_{1s}; the former was associated with Ti–O and the latter was attributable to In–O. Peaks at 531.4–531.9 eV indicated other oxygen species, possibly belonging to OH^- on the surface of the photocatalyst [32, 33]. The binding energy of Ti–O, In–O, and OH^- in Ti–In–C–N was 529.4, 529.7, and 531.6 eV (Fig. 2c). The binding energies of C_{1s}, which were 284.8, 285.4 and 288 eV, were attributed to C–C, C–O [34], and Ti–O–C [27] bonds (Fig. 2d). The 284.8 eV peak is due to the carbon-containing species adsorbed on the surface, which is usually ascribed to the adventitious carbon or carbon residues from the organic precursor [12]. Kang et al. [35] assigned the binding energy at 282 eV to the Ti–C bond that was formed by the substitution of carbon at an oxygen site in TiO_2; they assigned the binding energy at 288 eV to the presence of carbonate species that were formed by the substitution of carbon at the Ti site in TiO_2. The prepared Ti–In–C–N formed C–C and C–O bonds, but no Ti–C bonds. Chen et al. [11] reported that carbonate species that formed on the TiO_2
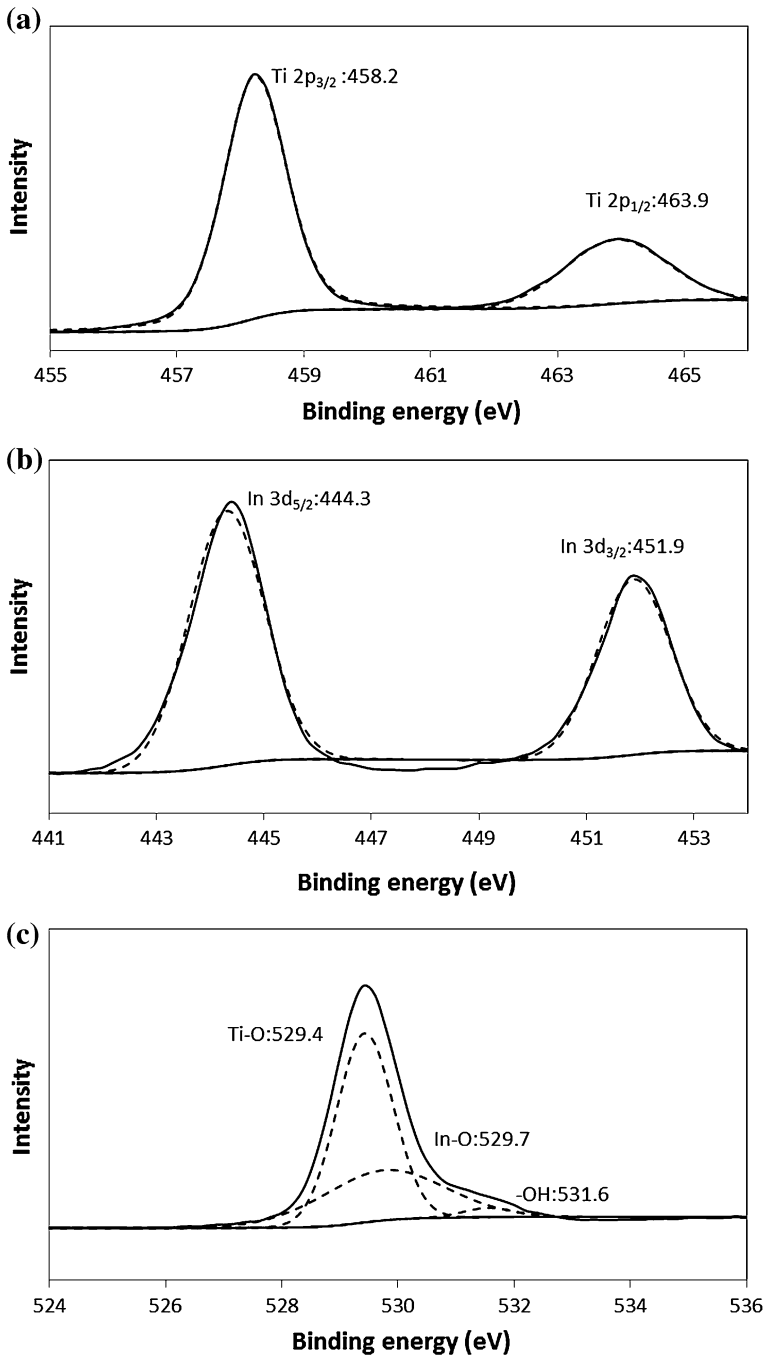
(a)

Ti 2p$_{3/2}$:458.2

Ti 2p$_{1/2}$:463.9

Intensity

Binding energy (eV)

(b)

In 3d$_{5/2}$:444.3

In 3d$_{3/2}$:451.9

Intensity

Binding energy (eV)

(c)

Ti-O:529.4

In-O:529.7

-OH:531.6

Intensity

Binding energy (eV)

Fig. 2 XPS spectra of Ti–In–C–N. **a** Ti$_{2p}$, **b** In$_{3d}$, **c** O$_{1s}$, **d** C$_{1s}$, **e** N$_{1s}$
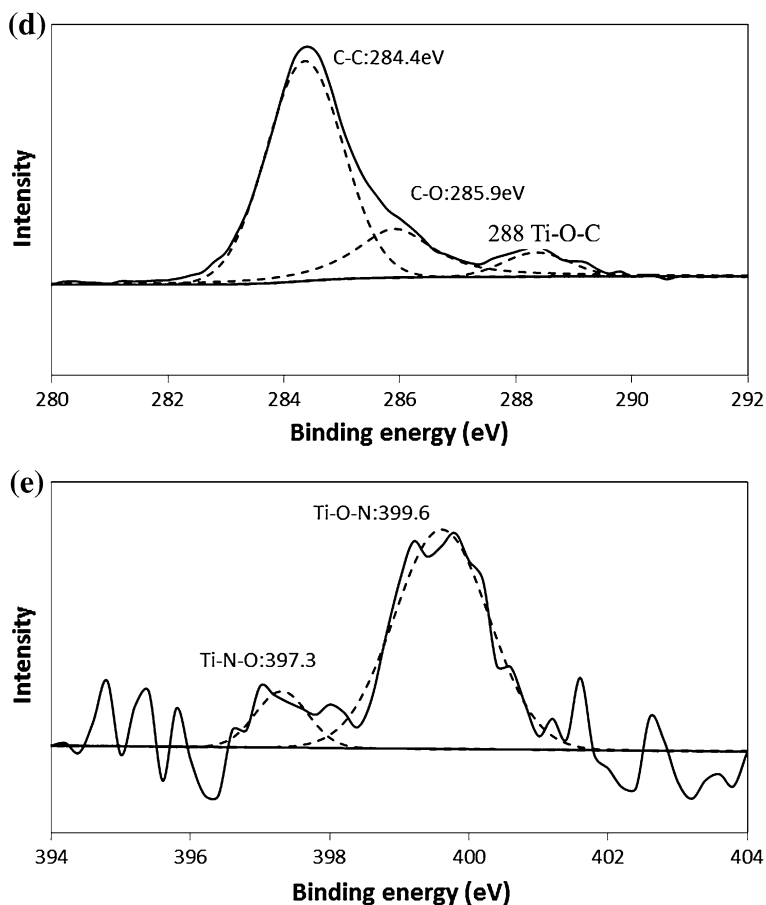
(d)

(e)

Fig. 2 continued

surface served as a photosensitizer, like an organic dye, promoting the absorption of TiO_2.

Fig. 3a–e present the XPS spectra of Ti_{2p}, In_{3d}, O_{1s}, N_{1s}, and S_{2p} for Ti–In–S–N. The XPS spectra of Ti_{2p}, In_{3d} and O_{1s} in Ti–In–S–N (Fig. 3a–c all revealed similar binding energies to those in Ti–In–C–N (Fig. 2a–c). Binding energies of 397.0–397.4 [36–38] and 398.6 eV [36, 37] in the N_{1s} region were assigned to Ti–N–O; the binding energy at 399–400.7 eV was attributed to the Ti–O–N bond [28, 31]. For Ti–In–C–N, Ti–N–O and Ti–O–N were obtained at the binding energy of 397.3 and 399.6 eV (Fig. 2e). Moreover, for Ti–In–S–N, Ti–N–O and Ti–O–N were obtained at the binding energy of 398.7 and 400 eV (Fig. 3d). The XPS spectra of Ti_{2p} and In_{3d} for Ti–In–C–N and Ti–In–S–N were similar to those for Ti–In [7] and Ti–In–N [39] ; moreover, the XPS spectra of O_{1s} and N_{1s} for Ti–In–C–N and Ti–In–S–N were similar to those obtained for Ti–In–N by Wu et al. [39] (data not
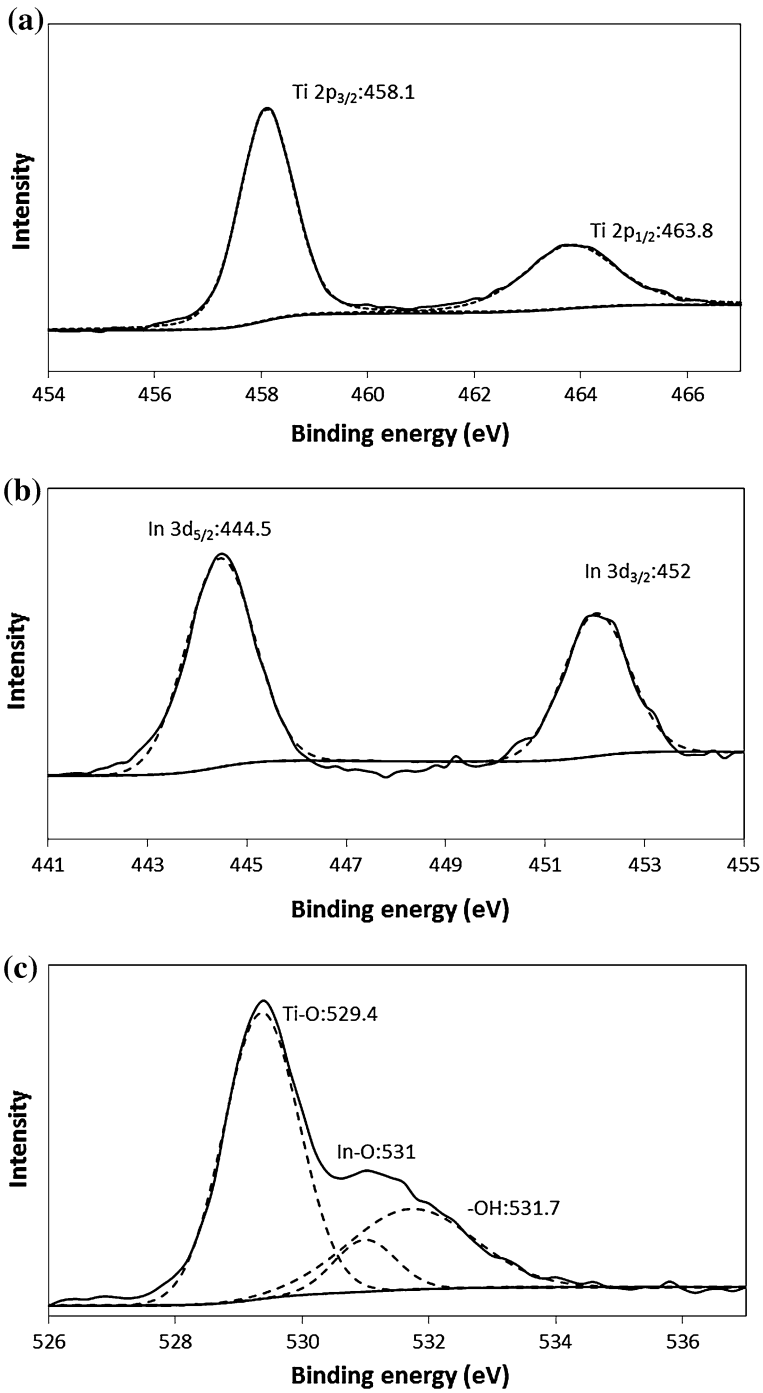
(a)

Ti 2p$_{3/2}$:458.1

Ti 2p$_{1/2}$:463.8

Intensity

454   456   458   460   462   464   466

Binding energy (eV)

(b)

In 3d$_{5/2}$:444.5

In 3d$_{3/2}$:452

Intensity

441   443   445   447   449   451   453   455

Binding energy (eV)

(c)

Ti-O:529.4

In-O:531

-OH:531.7

Intensity

526   528   530   532   534   536

Binding energy (eV)

Fig. 3 XPS spectra of Ti–In–S–N. **a** Ti$_{2p}$, **b** In$_{3d}$, **c** O$_{1s}$, **d** N$_{1s}$, **e** S$_{2p}$
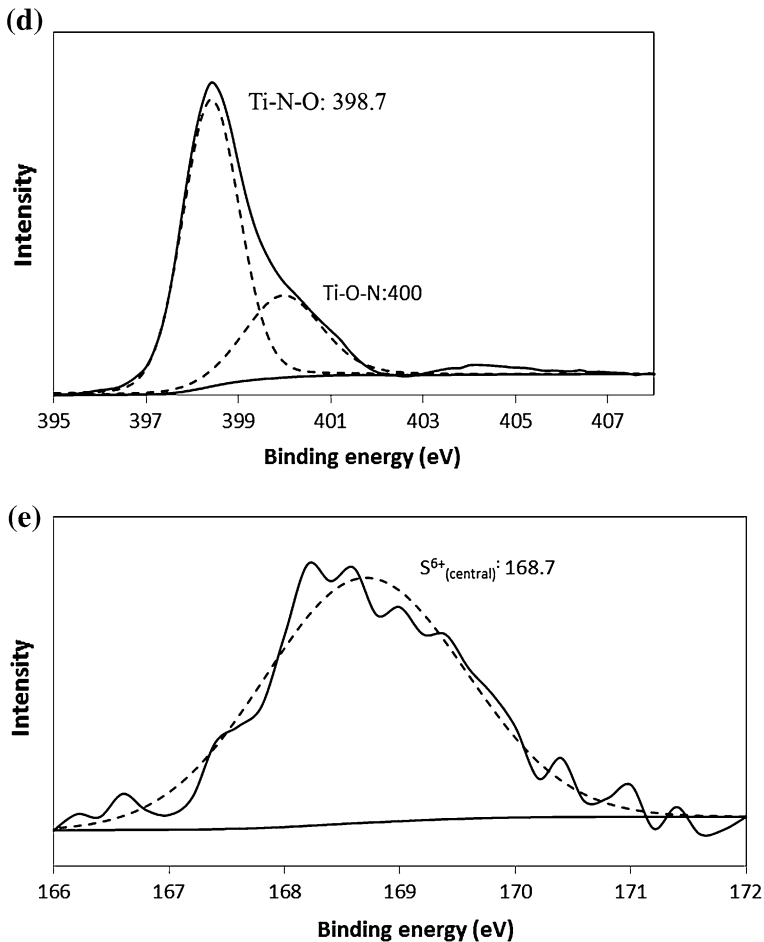
(d)

(e)

Fig. 3 continued

shown). Zhang et al. [40] indicated the post-nitridation of TiO_2 by NH_3 takes only place on the surface layer and sublayer of TiO_2 and maintains the original crystal phase of TiO_2 below 500 °C; accordingly, no crystalline phase of Ti–N was obtained. The present study identified two crystalline phases, Ti–O–N and Ti–N–O, which may be attributable to the use of urea rather than NH_3 as the precursor of N. Asahi et al. [24] utilized urea as a dopant and concluded that nitrogen atoms substituted at the lattice oxygen sites, forming an isolated narrow band above the valence band and narrowing the band gap. Notably, the preparation procedure varied among the studies cited above, and this variation may explain the various XPS observations.

The S atoms herein are in the S^{6+} state, yielding a peak at 168.2–169 eV [14, 16, 41]. The binding energy of S_{2p} in Ti–In–S–N is 168.7 eV (Fig. 3e). When S atoms
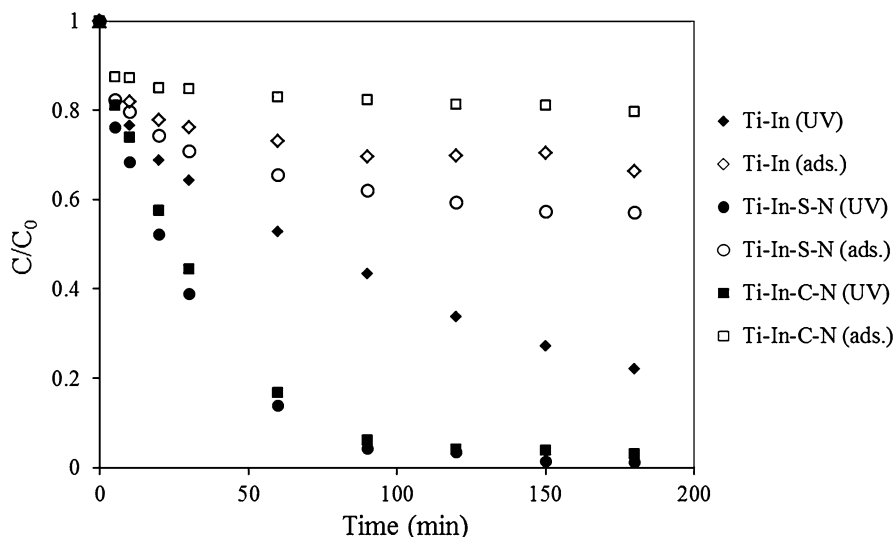
Fig. 4 RR2 removal in Ti–In, Ti–In–C–N and Ti–In–S–N systems via adsorption and photodegradation ([photocatalyst] = 0.2 g/L, [RR2] = 20 mg/L, pH 3)

replace O atoms on the TiO_2 surfaces, no peak in the range 160–163 eV, which corresponds to the Ti–S bond, is obtained [14]. Umebayashi et al. [42] suggested that sulfur was doped as an anion and replaced the lattice oxygen in TiO_2 to form Ti–S bond, conversely, Ohno et al. [41] reported that S atoms were incorporated as cations and replaced Ti ions in the S-doped TiO_2. Ho et al. [15] suggested that the oxidation state of the S-dopant depends on the preparation route. Anionic S doping may be difficult to perform because S^{2-} (0.17 nm) has a significantly larger ionic radius than does O^{2-} (0.122 nm). Hence, the substitution of Ti^{4+} by S^{6+} is chemically more favorable than replacing O^{2-} with S^{2-} [14], so Ti–In–S–N becomes positively charged. Therefore, the efficiency of adsorption of RR2 by Ti–In–S–N may exceed those of Ti–In–C–N and Ti–In.

Li et al. [18] found that the absorption spectra of S–N co-doped TiO_2 exhibited a red shift in the adsorption edge. This shift was attributed to the fact that calcination induces the doping of S and N atoms into the lattice of TiO_2, narrowing the band gap. Wang and Lim [26] observed a red shift of the absorption edge of C–N co-doped TiO_2 owing to the coexistence of Ti–C bonds, carbonate and oxynitride species in the TiO_2 lattice. The experimental results for Ti–In–C–N and Ti–In–S–N herein were similar to those for C–N co-doped TiO_2 and S–N co-doped TiO_2.

Photocatalytic properties of Ti–In, Ti–In–C–N and Ti–In–S–N

At pH 3, no significant decolorization occurred during direct photolysis (<5 %) (data not shown herein). Hence, the disappearance of RR2 was attributed to adsorption and/or photodegradation reactions. Fig. 4 presents the decolorization of RR2 by adsorption and photodegradation in different systems. After 180 min, the
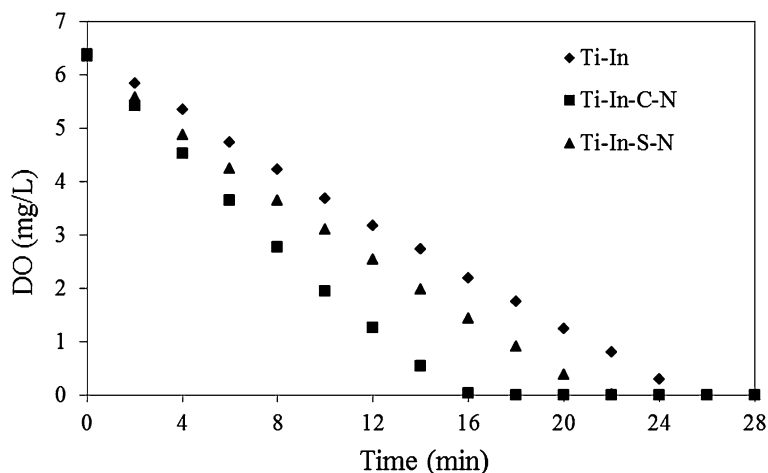
Fig. 5 DO uptake tests for RR2 effluent in in UV/Ti–In, UV/Ti–In–C–N and UV/Ti–In–S–N systems ([photocatalyst] = 0.2 g/L, [RR2] = 20 mg/L, pH 3)

adsorptions of RR2 (in the dark) by Ti–In, Ti–In–C–N and Ti–In–S–N were 34, 20 and 43 %, while the total removals of RR2 (adsorption and photodegradation under illumination) were 78, 97 and 99 %. Therefore, the net removal of RR2 that was attributable to photodegradation by various photocatalysts followed the order Ti–In–C–N > Ti–In–S–N > Ti–In. The order of RR2 adsorption by these photocatalysts was Ti–In–S–N > Ti–In > Ti–In–C–N, which agrees with the order of the surface areas of these photocatalysts. The removal of RR2 in all experiments followed pseudo-first order kinetics, as has been reported in various studies of RR2 decolorization [7, 13]. Table 1 lists the pseudo-first order RR2 removal rate constants (k), which follow the order Ti–In–S–N > Ti–In–C–N > Ti–In. The k values in UV/Ti–In, UV/Ti–In–N [39], UV/Ti–In–C–N, and UV/Ti–In–S–N were 0.43, 1.60, 1.68 and 1.70 h^{-1}. Clearly, the promotion of photocatalytic activity of Ti–In by co-doping with C–N or S–N was greater than that by N doping.

This study suggested that N atoms could form Ti–N–O and Ti–O–N, while C atoms could form a mixed layer deposited PAC and Ti–O–C bond at the surface of Ti–In–C–N particles. Furthermore, S atoms were incorporated as cations and replaced Ti ions in Ti–In–S–N. Based on the experimental analysis, C, S and N were successfully doped into Ti–In. The improved photocatalytic activity can be evidenced by an increase in either the number of Ti^{4+} defects or the number oxygen vacancies upon doping, the form of the impurity states, which inhibit the recombination of photogenerated hole and electron pairs, reduced band gap energy and increased lifetime of holes and electrons [43]. Yu et al. [17] suggested that the high activity of N–S co-doped TiO_2 can be attributed to the red shift of the adsorption edge, a large surface area and the two phase structures of N–S co-doped TiO_2. Large surface areas facilitate contact between holes (or electrons) and the pollutant molecules, improving photocatalytic activity.

Fig. 5 plots the DO profiles that were obtained by respirometric measurements of the RR2 effluent in different systems. The SOURs for the RR2 effluent (after 180 min reaction) in UV/Ti–In, UV/Ti–In–C–N and UV/Ti–In–S–N were determined to be 4.4, 7.3 and 5.3 mg O_2/g-MLVSS h. The C–N and S–N co-doped Ti–In improved the biodegradation of RR2 effluent. The enhancement of biodegradation by Ti–In–C–N exceeded that by Ti–In–S–N. The experimental results revealed that Ti–In–C–N effectively decolorized and detoxified RR2.

Conclusions

Novel Ti–In–C–N and Ti–In–S–N photocatalysts were fabricated in this study. C–N and S–N-co-doping in Ti–In inhibited the transformation of TiO_2 from anatase to rutile and particle agglomeration. The bang gap energy and particle diameter of Ti–In–C–N and Ti–In–S–N were smaller than those of Ti–In. The RR2 removal rates followed the order Ti–In–S–N > Ti–In–C–N > Ti–In. In this investigation, C, S and N were successfully doped into Ti–In, and the resulting improved photocatalytic activity was attributed to an increase in either the number of Ti^{4+} defects or the number of oxygen vacancies, which inhibited the recombination of photogenerated hole and electron pairs. Ti–In–C–N and Ti–In–S–N effectively decolorized and detoxified RR2.

References

1. Konstantinou IK, Albanis TA (2004) TiO₂-assisted photocatalytic degradation of azo dyes in aqueous solution: kinetic and mechanistic investigations—a review. Appl Catal B 49:1–14
2. Lo SC, Lin CF, Wu CH, Hsieh PH (2004) Capability of coupled CdSe/TiO₂ for photocatalytic degradation of 4-chlorophenol. J Hazard Mater 114:183–190
3. Ou XH, Wu CH, Lo SL (2006) Photodegradation of 4-chlorophenol by UV/photocatalysts: the effect of the interparticle electron transfer process. React Kinet Catal Lett 88:89–95
4. Lin CF, Wu CH, Onn SN (2008) Degradation of 4-chlorophenol in TiO₂, WO₃, SnO₂, TiO₂/WO₃ and TiO₂/SnO₂ systems. J Hazard Mater 154:1033–1039
5. Chakraborty AK, Rhaman MM, Hossain ME, Sobahan KMA (2014) Preparation of WO₃/TiO₂/In₂O₃ composite structures and their enhanced photocatalytic activity under visible light irradiation. Reac Kinet Mech Cat 111:371–382
6. Li C, Ming T, Wang J, Wang J, Yu JC, Yu SH (2014) Ultrasonic aerosol spray-assisted preparation of TiO₂/In₂O₃ composite for visible-light-driven photocatalysis. J Catal 310:84–90
7. Wu CH, Kuo CY, Lai CH, Chung WY (2014) Surface characteristics and photocatalytic properties of TiO₂-In₂O₃ composite powders by using the sol-gel method: effects of preparation conditions. Reac Kinet Mech Cat 112:543–557
8. Ma F, Zhang S, Yang X, Guo W, Guo Y, Huo M (2012) Fabrication of metallic platinum and indium oxide codoped titania nanotubes for the simulated sunlight photocatalytic degradation of diethyl phthalate. Catal Commun 24:75–79
9. Choi W, Termin A, Hoffmann MR (1994) The role of metal-ion dopants in quantum-sized TiO₂ - Correlation between photoreactivity and charge-carrier recombination dynamics. J Phys Chem B 98:13669–13679

10. Sojic DV, Despotovic VN, Abazovic ND, Comor MI, Abramovic BF (2010) Photocatalytic degradation of selected herbicides in aqueous suspensions of doped titania under visible light irradiation. J Hazard Mater 179:49–56

11. Chen D, Jiang Z, Geng J, Wang Q, Yang D (2007) Carbon and nitrogen co-doped TiO_2 with enhanced visible-light photocatalytic activity. Ind Eng Chem Res 46:2741–2746

12. Wang P, Yap PS, Lim TT (2011) C-N-S tridoped TiO_2 for photocatalytic degradation of tetracycline under visible-light irradiation. Appl Catal A 399:252–261

13. Kuo CY, Wu CH, Chen ST (2014) Decolorization of C.I. reactive red 2 by $UV/TiO_2/PAC$ and visible-light/TiO_2/PAC systems. Desalin Water Treat 52:834–843

14. Yu JC, Ho W, Yu J, Yip H, Wong PK, Zhao J (2005) Efficient visible-light-induced photocatalytic disinfection on sulfur-doped nanocrystalline titania. Environ Sci Technol 39:1175–1179

15. Ho W, Yu JC, Lee S (2006) Low-temperature hydrothermal synthesis of S-doped TiO_2 with visible light photocatalytic activity. J Solid State Chem 179:1171–1176

16. Liu SY, Tang QL, Feng QG (2011) Synthesis of S/Cr doped mesoporous TiO_2 with high active visible light degradation property via solid state reaction route. Appl Surf Sci 257:5544–5551

17. Yu J, Zhou M, Cheng B, Zhao X (2006) Preparation, characterization and photocatalytic activity of in situ N, S-codoped TiO_2 powders. J Mol Catal A 246:176–184

18. Li X, Xiong R, Wei G (2008) S-N co-doped TiO_2 photocatalysts with visible-light activity prepared by sol-gel method. Catal Lett 125:104–109

19. Yang X, Wang Y, Xu L, Yu X, Guo Y (2008) Silver and indium oxide codoped TiO_2 nanocomposites with enhanced photocatalytic activity. J Phys Chem C 112:11481–11489

20. Spurr RA, Myers H (1957) Quantitative analysis of anatase-rutile mixtures with an Xray diffractometer. Anal Chem 29:760–762

21. Klug P, Alexander LE (1974) X-ray diffraction procedures. Wiley, New York

22. Hurum DC, Agrios AG, Gray KA, Rajh T, Thurnauer MC (2003) Explaining the enhanced photocatalytic activity of degussa P25 mixed-phase TiO_2 using EPR. J Phys Chem B 107:4545–4549

23. Li Y, Zhang S, Yu Q, Yin W (2007) The effects of activated carbon supports on the structure and properties of TiO_2 nanoparticles prepared by a sol–gel method. Appl Surf Sci 253:9254–9258

24. Asahi R, Morikawa T, Ohwaki T, Aoki K, Taga Y (2001) Visible-light photocatalysis in nitrogen-doped titanium oxides. Science 293:269–271

25. Min Y, Zhang K, Zhao W, Zheng F, Chen Y, Zhang Y (2012) Enhanced chemical interaction between TiO_2 and grapheme oxide for photocatalytic decolorization of methylene bule. Chem Eng J 193–194:203–210

26. Wang X, Lim TT (2011) Effect of hexamethylenetetramine on the visible-light photocatalytic activity of C-N codoped TiO2 for bisphenol A degradation: evaluation of photocatalytic mechanism and solution toxicity. Appl Catal A 399:233–241

27. Xiao Q, Ouyang L (2009) Photocatalytic activity and hydroxyl radical formation of carbon-doped TiO_2 nanocrystalline: Effect of calcination temperature. Chem Eng J 148:248–253

28. Sasikala R, Shirole AR, Sudarsan V, Jagannath Sudakar C, Naik R, Rao R, Bharadwaj SR (2010) Enhanced photocatalytic activity of indium and nitrogen co-doped TiO_2-Pd nanocomposites for hydrogen generation. Appl Catal A 377:47–54

29. Wang X, Hu Z, Chen Y, Zhao G, Liu Y, Wen Z (2009) A novel approach towards high performance composite photocatalyst of TiO_2 deposited on activated carbon. Appl Surf Sci 255:3953–3958

30. Tominaga M, Hirata N, Taniguchi I (2005) UV-ozone dry-cleaning process for indium oxide electrodes for protein electrochemistry. Electrochem Commun 7:1423–1428

31. Reyes-Gil KR, Reyes-Garcia EA, Raftery D (2007) Nitrogen-doped In_2O_3 thin film electrodes for photocatalytic water splitting. J Phys Chem C 111:14579–14588

32. Eshaghi A, Pakshir M, Mozaffarinia (2010) Preparation and photo-induced superhydrophilicity of composite TiO_2–SiO_2–In_2O_3 thin film. Appl Surf Sci 256:7062–7066

33. Zheng J, Liu Z, Liu X, Yan X, Li D, Chua W (2011) Facile hydrothermal synthesis and characteristics of B-doped TiO_2 hybrid hollow microspheres with higher photo-catalytic activity. J Alloy Compd 509:3771–3776

34. Le HA, Linh LT, Chin S, Jurng J (2012) Photocatalytic degradation of methylene blue by a combination of TiO_2-anatase and coconut shell activated carbon. Powder Technol 225:167–175

35. Kang IC, Zhang Q, Yin S, Sato T, Saito F (2008) Preparation of a visible sensitive carbon doped TiO_2 photo-catalyst by grinding TiO_2 with ethanol and heating treatment. Appl Catal B 80:81–87

36. Saha NC, Tompkins HG (1992) Titanium nitride oxidation chemistry: An x-ray photoelectron spectroscopy study. J Appl Phys 72:3072–3079

37. Gyorgy E, Pino AP, Serra P, Morenza JL (2003) Depth profiling characterisation of the surface layer obtained by pulsed Nd:YAG laser irradiation of titanium in nitrogen. Surf Coat Technol 173:265–270
38. Ismail IM, Abdallah B, Abou-Kharroub M, Mrad O (2012) XPS and RBS investigation of TiN_xO_y films prepared by vacuum arc discharge. Nucl Instrum Method Phys Res B 271:102–106
39. Wu CH, Kuo CY, Wu JT, Hong PKA, Lai CH, Chung WY (2014) Effects of nitrogen and carbon dopings on properties and photocatalytic activity of TiO_2–In_2O_3 composite. Korean J Chem Eng (revised)
40. Zhang Z, Wang X, Long J, Gu Q, Ding Z, Fu X (2010) Nitrogen-doped titanium dioxide visible light photocatalyst: Spectroscopic identification of photoactive centers. J Catal 276:201–214
41. Ohno T, Akiyoshi M, Umebayashi T, Asai K, Mitsui T, Matsumura M (2004) Preparation of S-doped TiO_2 photocatalysts and their photocatalytic activities under visible light. Appl Catal A 265:115–121
42. Umebayashi T, Yamaki T, Yamamoto S, Miyashita A, Tanaka S, Sumita T, Asai K (2003) Sulfur-doping of rutile-titanium dioxide by ion implantation: photocurrent spectroscopy and first-principles band calculation studies. J Appl Phys 93:5156–5160
43. Lu X, Tian B, Chen F, Zhang J (2010) Preparation of boron-doped TiO_2 films by autoclaved-sol method at low temperature and study on their photocatalytic activity. Thin Solid Films 519:111–116